E. coli division machinery drives cocci development inside host cells

Alaska Pokhrel[1,*], Ariana Costas[1,2], Matthew Pittorino[1], Iain Duggin[1] and Bill Söderström[1,*]

[1] Australian Institute for Microbiology and Infection
University of Technology Sydney
2007 Ultimo, Australia

[2] Institut Cochin,
INSERM U1016, CNRS UMR 8104,
Paris 75014, France.

* Address correspondence to:
Bill Söderström: Bill.soderstrom@uts.edu.au Tel: +61 2 9514 4970
Alaska Pokhrel: Alaska.pokhrel@uts.edu.au Tel: +61 2 9514 4970

Abstract

We show Uropathogenic *E. coli* rods dividing to form and proliferate as cocci inside host cells. In these intracellular bacterial communities, the frequency of cell division outpaced the rate of cell growth, resulting in smaller cocci cells. This mechanism was guided by an active FtsZ-governed division machinery, directed to midcell by division-site placement systems. These results show how a previously uncharacterised level of morphological plasticity occurs in bacteria with traditionally well-defined rod shape.

Main

During unfavourable environmental conditions, bacteria can modulate growth and division as a survival strategy [1]. One striking example of this is the typically rod-shaped Uropathogenic *Escherichia coli* (UPEC) that during urinary tract infections (UTI) morphs into both cocci and filamentous morphologies [2]. UTI are one of the strongest drivers of antimicrobial resistance worldwide [3], where UPEC accounts for some 75-80% of all reported cases [2], and while the overall infection cycle is largely mapped [4], surprisingly few molecular details of the intracellular lifecycle of UPEC during UTI are currently known.

UPEC invasion of human epithelial bladder cells results in densely packed colonies of bacteria known as intracellular bacterial communities (IBC) [5,6], with a substantial amount of bacteria appearing as cocci with cell lengths around 1 μm or less [7]. It was previously hypothesised that these cells simply slowly "shrank" or "transitioned" into cocci [7,8]. Nutrient depletion was not considered a growth limiting factor as the bacterial biomass increased over time, with generation times exceeding 60 min once inside the bladder cells [9]. However, the basic mechanism for apparent cocci cell formation in intracellular UPEC has remained unknown. Here, we visualised bacterial proliferation and subcellular structures inside cultured human bladder cells and identified the bacterial cell division machinery, 'the divisome', and its regulatory systems as key players in cocci formation and proliferation.

We used an UTI *in-vitro* infection model where a layer of immortalized human epithelial bladder cells is challenged with UPEC (Supplementary fig. 1) [10,11]. Bacterial division dynamics were followed inside the bladder cells using live cell fluorescence microscopy (Fig. 1a). Roughly 6h post infection [7], UPEC rod-to-cocci transitions occurred with only one or a few cells present in the bladder cell cytoplasm (Fig. 1b). This observation partly contrasts previous studies stating that cocci formation is only initiated in dense IBCs, albeit in a different model system at lower time resolution [7].
As expected, intracellular bacteria were overall significantly shorter than extracellular bacteria, 1.3 ± 0.53 μm (n = 100) and 2.59 ± 0.41 μm (n = 117) respectively (Fig. 1c), with an overall smaller area: $Area_{Intra}$ 0.91 ± 0.54 μm^2 (n = 100) vs $Area_{Extra}$ 2.32 ± 0.43 μm^2 (n = 117) (Fig. 1d). Following division dynamics of intracellular bacteria over time (average length before division 1.84 ± 0.31μm (n = 44), we saw that rods divided into coccoid shape with average lengths of 0.88 ± 0.13 μm (n = 56) (Fig. 1e - f), often with an aspect ratio close to 1 (average 1.3 ± 0.19, Fig. 1g). This was significantly different from the aspect ratio of extracellular cells after division 2.13 ± 0.13 (n = 76) (Supplementary fig. 2). These cocci subsequently divided into new cocci (Supplementary fig. 3, Supplementary movie SM2). To see if this division behaviour was more broadly adapted by UPEC, we ran another clinical urinary tract isolate, MS2027 [12], in the infection model. Division patterns and times of intracellular rods dividing into cocci of MS2027 were indistinguishable from those of UTI89 (Supplementary fig. 4). Taken together, our data clearly shows that intracellular UPEC actively divide into cocci, and is maintained as cocci through multiple generations.

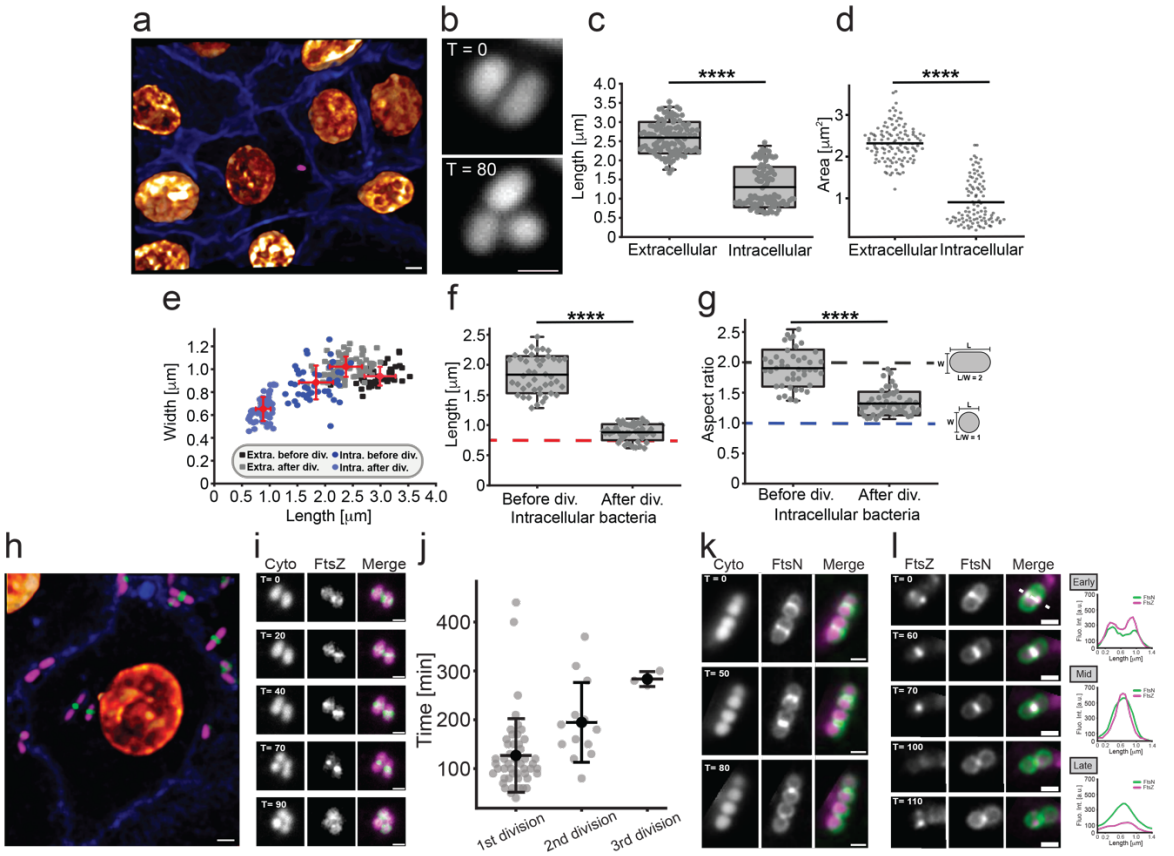

Figure 1. UPEC rod-to-cocci divisions during infection are governed by the divisome. ***a****, PD07i human epithelial bladder cells (membranes blue, nuclei gold) were challenged with fluorescently labelled UPEC (magenta). All subsequent images show intracellular bacteria* ***b****, Representative images of cells before (T = 0) and after division (T = 80), note that one daughter cell has left the field of view.* ***c - d****, Average cell length (****c****) and area (****d****) of extracellular and intracellular bacteria.* ***e****, Length vs width of extracellular ('Extra') and intracellular ('Intra') bacteria.* ***f - g****, Lengths (****f****) and aspect ratio (****g****) of intracellular bacteria before and after division. Red dotted line represents average cocci width after division.* ***h****, Representative image of intracellular UPEC expressing a division marker (FtsZ-mCitrine) with mCherry as cytoplasmic marker.* ***i****, Still images of a time-lapse sequence showing FtsZ-mCitrine driven cocci divisions (Supplementary movie SM3).* ***j****, Average division times of intracellular bacteria.* ***k****, mCitrine-FtsN midcell constriction during cocci divisions (Supplementary movie SM4).* ***l****, FtsZ-mCherry and mCitrine-FtsN dynamics during cocci divisions. Fluorescence intensity plots high-light a larger radius of FtsN (Mid, T = 70) and that it remains longer at septum than FtsZ (Late, T = 100). Statistical significance was determined by student's T-test, where **** stars indicate p values less than 0.0001. Box plots: box edge equals S.D., midline represents average, and whiskers indicate 1-99% interval. Times are in minutes. Scale bars a = 4 µm; b, i, k & l = 1 µm; h = 2 µm.*

To substantiate our observation that cocci formation is driven by cell division, we followed divisome dynamics in UTI89 expressing fluorescent division markers (FtsZ-mCitrine and/or mCitrine-FtsN) during intracellular divisions (Fig. 1h, 1i and 1k). The central bacterial division protein FtsZ forms the characteristic "Z-ring" at the onset of division [13]. Using Z-ring accumulation at midcell as a marker for on-going division,

cocci division times ranged from roughly 50 minutes up to more than two hours (Mean: 127 ± 75 min, n = 49), and beyond 6 hours in the extreme case (Fig. 1i-j), overall, far greater than the ~ 20 min generation times in growth media (Supplementary fig. 5). FtsZ dynamics in MS2027 were similar to those in UIT89 (Supplementary fig. 4). When following the same cocci over multiple generations, we observed that the average division time since previous division increased: 2nd division average time 195 ± 81 min (n = 13) and 3rd division average time 283 ± 15 min (n = 3, note only few cells could be followed over multiple generations due to the challenging 3D imaging environment) (Fig. 1j). Intracellular mCitrine-FtsN dynamics indicated similar division times (Fig. 1k).

FtsZ and FtsN (the first and the last essential division protein to assemble at division sites, respectively) localization dynamics followed the same constriction patterns in cocci as in rods where FtsZ-mCherry had apparent smaller radii compared to mCitrine-FtsN during constriction (Fig. 1l, "mid") [14], with FtsZ-mCherry disassembling from the division site prior to mCitrine-FtsN towards the end of division (Fig. 1l, Supplementary movie SM5). Based on these data, we conclude that the divisome is actively dividing rods into cocci, with key components of the divisome following similar localization dynamics as in vegetative growth [15]. Deleting genes implicated in regulating division and morphology during UTI (*e.g.*, *sulA*[16], *ymfM*[17], *damX*[18]) did not result in observable changes in the rod to cocci transitions (Supplementary fig. 6).

The above presented findings presented an interesting conundrum, how does a normally rod-shaped cell know where to place the cell division machinery when being round? In UPEC rods, the division machinery is guided to midcell by MinC concentration minima generated by pole-to-pole oscillations of Min system[19]. However, simulations and experiments have suggested that short rods below a certain length (~ 2.5 μm or less) do not exhibit smooth MinD oscillations, and show no oscillations or rather stochastic pole-to-pole switching [20]. Here, we examined EYFP-MinD dynamics in intracellular cocci (Fig. 2a), which revealed a concentration minimum at midcell both from pole-to-pole oscillations and from apparent circumferential movements along the cell perimeter (Fig. 2b – c, Supplementary movie SM6). As in rods, FtsZ-rings were observed at the EYFP-MinD concentration minima, and always in the same plane Z-rings from previous divisions, suggesting a maintained polarity also in cocci (Fig. 2d). The average EYFP-MinD oscillation speed normalized to cell length was significantly lower in intracellular bacteria: 0.055 μm sec^{-1}, compared to 0.094 μm sec^{-1} for extracellular bacteria (Fig. 2e - f). Furthermore, in shorter cells, roughly shorter than 1.3 μm (much less than the 2.5 μm previously predicted), we noticed that the typical pole-to-pole oscillations broke down and were replaced by more complex dynamics, such as circular movements along the circumference and stochastic transitions from one pole to the other (Fig. 2g)

Deletion of the Min system is known to generate 'mini-cells' often devoided of genetic material [21,22]. To investigate whether UPEC cocci had DNA and whether the nucleoid occlusion mechanism to prevent division over the DNA [23] was preserved during intracellular rod-to-cocci divisions, we looked at UPEC chromosome segregation in host cells over time. Imaging intracellular UTI89 expressing a DNA marker (HupA-RFP), we never observed a cell division where the DNA did not partition into both daughter cocci (Fig. 2h). Global DNA partitioning in cocci was efficient (Fig. 2i), indistinguishable to what has been found in rods previously [24]. The average nucleoid length in intracellular cocci was 0.79 ± 0.12 μm (n = 100), while for extracellular cells

it was 1.45 ± 0.2 μm (n = 216) (Fig. 2j - k). When we co-observed DNA segregation (HupA-RFP) and septal constriction (FtsZ-mNeonGreen) in the same cells (Supplementary fig. 7), we observed that FtsZ-rings readily formed over unsegregated nucleoids and appeared to initiate constriction prior to observable chromosome segregation in cocci (Fig. 2l - m). FtsZ ring radius decreased up to ~ 140 nm prior to visible HupA-RFP intensity decrease at midcell (Fig. 2m). As the nucleoid occlusion regulator *slmA* controls chromosome partitioning in rods during vegetative growth, we further looked at chromosomes (HupA-RFP) and Z-rings (FtsZ-mNeonGreen) in UTI89Δ*slmA* cocci during infection (Fig. 2n). Z-rings initiated constriction over incompletely segregated nucleoids in Δ*slmA* cocci at a slightly larger degree than in WT, 85.3 (± 9.6) vs 72 (± 6.55) % of cells respectively, but with a non-statistically significant difference (p = 0.118) (Fig. 2o). In contrast to intracellular UPEC, FtsZ-mNeonGreen in extracellular rods constricted only when chromosomes were visibly separated (Fig. 2p), even in short cells ~ 2 - 2.5 μm just after previous divisions (Supplementary movie SM7).

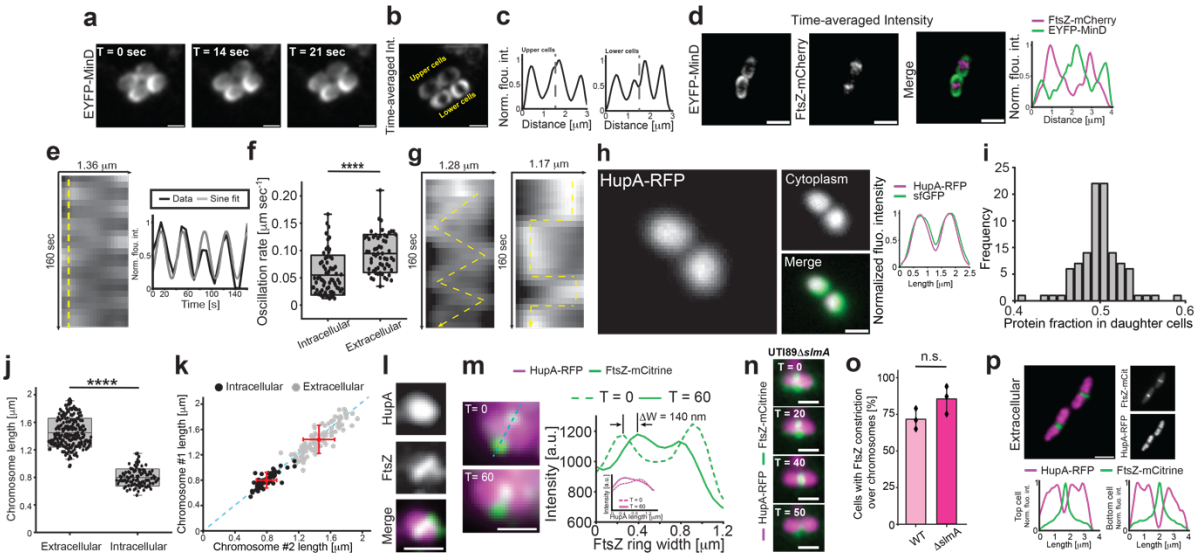

Figure 2. Functions of division site placement systems in UPEC cocci division during infection.

***a**, Still images from an EYFP-MinD time-lapse series showing dynamics in intracellular UTI89 cocci (Supplementary movie SM6). **b - c**, Time-averaged fluorescence intensity of EYFP-MinD. Dotted line in plots represent cell boundaries. **d**, Time-averaged fluorescence intensity of EYFP-MinD and FtsZ-mCherry, indicating that FtsZ localize at MinD minima in cocci. **e**, Typical kymograph of EYFP-MinD oscillations of a cell longer than 1.3 μm. Yellow dotted line represents where intensity plot was drawn. **f**, Average EYFP-MinD oscillation rate in intracellular bacteria was 0.055 ± 0.036 μm sec^{-1} (n = 71) and in extracellular 0.095 ± 0.035 μm sec^{-1} (n = 60) cells. **g**, Typical kymographs of EYFP-MinD oscillations of cells shorter than 1.3 μm show complex non-standard pole-to-pole oscillation dynamics. Kymographs generated from the two lower cells in Supplementary movie SM6. **h - i**, DNA (HupA-RFP) partitioning in cocci (msfGFP as cytoplasmic marker). DNA segregates equally into daughter cocci. n = 98. **j**, Average chromosome lengths in extracellular (n = 216) and intracellular bacteria (n = 98). **k**, Chromosomes partitions into equal size after division in both extracellular (grey) and intracellular (black) bacteria. Blue dashed line indicates linear dependence. Red dots indicate average, with x-y bars representing S.D. **l - n**, FtsZ-mNeonGreen*

rings assemble and, partly, constricts over undivided chromosomes (HupA-RFP) in both WT and ∆slmA cocci. Intensity plot in ***m*** *shows FtsZ constriction over 60 min (inset show HupA-RFP fluorescence profiles with no intensity decrease at midcell). Cerulean dotted line indicate from where intensity plot is generated.* ***o,*** *Level of FtsZ-mNeonGreen constriction over unsegregated chromosomes. Averages of more than 30 cells from 3 independent infections.* ***p****, FtsZ-mNeonGreen rings do not constrict over undivided chromosomes in extracellular rods. Statistical significance was determined by student's T-test, where **** stars indicate p values less than 0.0001. n.s. = not significant. Box plots: box edge equals S.D., midline represents average, and whiskers indicate 1-99% interval. Times are in minutes. Scale bars a, b, h, l, m and n = 1 μm; d and p = 2 μm.*

Here, we show that rod-shaped bacteria actively divide into smaller cocci and maintain such morphology over several generations while in an intracellular environment. This morphology change is achieved by an active cell division machinery, with protein dynamics like those in binary fission of rod-shaped cells during vegetative growth. The cell division machinery and Min oscillations in spherically shaped *E. coli* cells previously has been investigated in mutant strains under in vitro conditions [25]. But to our knowledge, present study is the first time this phenomenon has been experimentally investigated as a wild-type mode of proliferation. Cocci-based FtsZ and FtsN constriction patterns were similar to those in rods, but interdivision times were on average six times larger. MinD dynamics were slower in cocci, and pole-to-pole transitions were found to switch from continuous oscillations to stochastic with decreasing cell size. While chromosome partitioning was maintained during cocci division, FtsZ constriction was initiated prior to visual nucleoid segregation suggesting a less pronounced SlmA activity in this type of divisions.

One plausible reason for UPEC to divide into cocci shape could be to allow for a higher number of bacteria per infected bladder cell, up to two orders of magnitude more than for unorganised bacilli [26], or greater compaction of bacteria in IBCs. UPEC cocci have shown a survival advantage over rods within intestine in murine models[8]. Based on that deletions of SOS and other genes related to filament regulation does not affect cocci division dynamics, combined with increased interdivision times, we speculate that UPEC rod-to-cocci morphology changes are largely a result of the low nutrient availability in the hostile environment presented during intracellular life in human bladder cells.

Methods

Bacteria growth and protein production

Bacterial strains used throughout the study were routinely plated on LB agar (Difco) plates supplemented with appropriate antibiotics (Ampicillin: 100 μg ml^{-1} (Sigma), Spectinomycin 100 μg ml^{-1} (Sigma), Kanamycin 50 μg ml^{-1} (Sigma), Chloramphenicol 25 μg ml^{-1} (Sigma)). A single colony of respective *E. coli* strain was grown in LB media (Difco) supplemented with appropriate antibiotics at 37°C overnight without shaking. Following overnight growth, cultures were were pelleted and resuspended in 1x PBS (Bio-Rad) to an optical density (OD_{600}) of 0.1. Fluorescent protein fusion production was initiated by addition of 1μM IPTG for FtsZ-mCitrine (pHC054) in UTI89 (2μM IPTG in MS2027), 5μM IPTG for EYFP-MinD (pSR-4) and HupA-RFP (pSTC011), and 15μM Rhamnose for mCitrine-FtsN (pHC004). Note that FtsZ-mNeonGreen (pMP7), FtsZ-mCherry (pMP11), sfGFP (pGI5) and mCherry (pGI6) did not require induction as they are produced under constitutive promoters. Viability, generation times and cell dimensions were comparable to a those of a WT strain grown under the same conditions (Supplementary fig. 5). Bacterial strains and plasmids used in this study are listed in Supplementary table 1.

Cell culture

Immortalized human epithelial bladder cells PD07i[27] were maintained in antibiotic free growth EpiLife Medium (Gibco) supplemented with growth supplement (HKGS) at 37°C in the presence of 5% CO_2. Cells were passaged using standard trypsinization protocols upon reaching ~ 75 - 90% confluency. To prepare for infection, cells were seeded in 35 mm glass bottom petri-dishes (IBIDI, #1.5H glass, Cat.No:81158) and grown to confluency.

Infection model

Seeded petri-dishes were challenged with appropriate bacterial strain at an MOI of ~ 100 (roughly corresponding to 10^7 cells as determined by CFU counts). To facilitate increased bacterial adherence to the bladder cells, dishes were spun at 500 rpm for 3 minutes, before incubation at 37°C (5% CO_2) with orbital agitation (50 rpm) for 15 minutes. Media containing bacteria was removed and the petri-dishes were replenished with fresh pre-warmed EpiLife media supplemented with inducer as appropriate. Dishes were incubated for at least 6 hours to let bacteria invade the bladder cells and initiate intracellular divisions (which coincides with “middle IBC” maturation[7]). Following incubation, media was removed from petri-dish and cells were washed once with 1 x PBS. The bladder cells were stained for membrane (CellBrite Steady Membrane 405) and nucleus (NucSpot Live Cell 650) for 30 minutes in pre-warmed EpiLife as per manufacturer’s instructions (Biotium, San Francisco, USA). After the staining step and two washes with 1 x PBS, cells were covered in fresh pre-warmed EpiLife (supplemented with inducer as required) and Gentamicin f.c. 50 μg ml^{-1} (Sigma) and taken for imaging. Only intracellular bacteria survive this standard Gentamycin protection assay treatment[28], and thus dividing bacteria are inside bladder cells (Supplementary movie SM1) while non-dividing bacteria are extracellular (Supplementary movie SM8). Generally, all infection experiments were run in at least three independent replicates, unless otherwise indicated.

Imaging

For time-lapse imaging, live cells were imaged in the glass bottom petri dishes on a Nikon N-STORM v5 TiE2 (with NIS v.5.30) microscope in TIRF mode using HILO illumination, with a 100 x 1.49 NA oil objective, to increase the signal-to-noise ratio. To support live cell imaging, the microscope was equipped with a stage top environmental chamber regulating temperature (37°C) and CO_2 levels (5% CO_2). 405, 488, 561 and 647 nm laser lines were used to excite fluorescent probes (405: membrane dye. 488: mCitrine, mNeonGreen, EYFP. 561: mCherry. 647: nuclear dye) as appropriate. Acquisition times were 70-400 ms and image size 2048 x 2048 (pixel size 65 nm). Fluorescence emission was collected via emission filters sets for DAPI, FITC, TxRed and 'Normal STORM(647)'. Images were captured using a sCMOS Flash 4.0 v3 (Hamamatsu) camera. To follow the bacterial cell division within live bladder cells, images were acquired every 7 - 10 minutes for at least 6 hours (Note: it was generally not possible to accurately track more than 1 division event due to the intracellular movements with bacteria transitioning in and out of focus). To follow short term EYFP-MinD dynamics, images were acquired every 5 - 7 seconds for at least 2 minutes.

For confocal live cell imaging, images were acquired on a Leica Stellaris 8 confocal microscope equipped with a 63x NA1.49 oil objective enclosed in an environmental chamber at 37°C in the presence of 5% CO_2. Fluorophores were excited using a white laser, and emission was collected using software optimized settings in the LAS software. Image size was chosen to either 2048 x 2048 or 4096 x 4096 pixels, with individual pixel size 90 and 45 nm, respectively. The pinhole was set to 1 AU and Z-stacks were collected with step length of either 125 or 250 nm (15 - 99 images per stack, depending on step length and thickness of the bladder cell in question).

Image postprocessing

Raw microscopy images were transferred to Fiji for processing and analysis. Time-lapse image sequences were drift-corrected using StackReg or HyperStackreg where appropriate, and background was subtracted using a rolling ball radius of 50. Images were denoised using the PureDenoise plug-in. To follow division of intracellular bacteria/cocci (Fig. 1 b-g), time-lapse sequences were segmented based on cytoplasmic fluorescent protein intensity using the tracking work-flow in the ilastik Fiji plug-in (version 1.4.0). Divisions were determined being over at the time point of the first image of visually separated cells. EYFP-MinD based kymographs were generated using KymoResliceWide. Time-averaged fluorescence intensity images of EYFP-MinD were generated using the standard deviation option in the Z-projection tab. Deconvolution and reconstruction of confocal Z-stacks were performed using Leica LAS.

Data analysis and statistics

Cell length, area, aspect ratio, and chromosome length of intra- and extra-cellular cells (rods and cocci) were extracted by using the MicrobeJ [29] plug-in or from manually traced dimensions in Fiji. Intracellular UPEC expressing fluorescent protein fusions to a division protein were followed for 1 - 3 divisions in time-lapse movies to manually extract intracellular division times. Visible FtsZ-FP accumulation at midcell was taken as initiation of division, and its disassembly from midcell was taken as completed division. Generally, fluorescence intensity profiles were generated in Fiji and analysed in Origin Pro 2021 Academic (V9.8.0.200). EYFP-MinD oscillation rates per length in intra- and extra-cellular cells were determined by measuring cell lengths and

extracting fluorescence profiles over time generating corresponding kymographs. Statistical analysis were performed in either Origin Pro 2021 Academic or GraphPad Prism 10 (V10.0.3). Statistical significance was datamined by student's T-test, where **** stars indicate p values less than 0.0001, unless defined otherwise. Figures were prepared using Adobe Illustrator.

Western blotting

A culture volume corresponding to 0.1 OD units was collected from each UPEC strain expressing the protein of interest after at least 6 hours of growth in PD07i seeded petri-dishes (Supplementary fig. 5). The samples were pelleted and re-suspended in SDS-loading buffer and resolved by SDS-PAGE gel electrophoresis. Proteins of interest (FtsZ, FtsN and MinD) were transferred to nitrocellulose membranes using a semi-dry Transfer-Blot apparatus (Bio-Rad). The Nitrocellulose membranes were then blocked in 5% (w/v) skim milk and probed with the respective primary (anti-FtsZ, Agrisera. Anti-FtsN [30]. Anti-MinD antisera, gift from Dr. Yu-ling Shih, Academia Sinica, Taiwan. All primary antibodies were used at 1:3333) and secondary antibody (anti-rabbit HRP, 1:10000, Bio-Rad) before washed and imaged (GE Amersham Imager 600).

Acknowledgments
The authors wish to acknowledge members of Australian Institute for Microbiology and Infection, AIMI, at UTS for discussions and suggestions on the manuscript.
Work in the Söderström lab is funded by the Australian Research Council through an ARC Discovery Project grant (DP220101143). B.S. is supported by an ARC Future Fellowship (FT230100062). A.P. acknowledges the UTS Faculty of Science for a seed funding grant. The authors further wish to acknowledge the use of Nikon N-STORM and Leica Stellaris 8 confocal microscopes within the Microbial Imaging Facility in the Faculty of Science at the University of Technology Sydney.

Author Contributions
A.P and B.S conceptualized the study. A.P, A.C and B.S. performed the experiments. A.P and B.S analysed the data with input from I.D.
A.C and M.P contributed reagents. A.P, B.S wrote the manuscript, with editorial input from all authors. All authors approved the final version of the manuscript.

Conflict of interest
The authors declare no conflicts of interest.

Data availability

All data are presented in the main figures and in the supplementary information.

Code availability
No new code was generated in this study.

References

1 Justice, S. S., Hunstad, D. A., Cegelski, L. & Hultgren, S. J. Morphological plasticity as a bacterial survival strategy. *Nat Rev Microbiol* **6**, 162-168, doi:10.1038/nrmicro1820 (2008).

2 Flores-Mireles, A. L., Walker, J. N., Caparon, M. & Hultgren, S. J. Urinary tract infections: epidemiology, mechanisms of infection and treatment options. *Nat Rev Microbiol* **13**, 269-284, doi:10.1038/nrmicro3432 (2015).

3 Antimicrobial Resistance, C. Global burden of bacterial antimicrobial resistance in 2019: a systematic analysis. *Lancet* **399**, 629-655, doi:10.1016/S0140-6736(21)02724-0 (2022).

4 Abell-King, C., Costas, A., Duggin, I. G. & Söderström, B. Bacterial filamentation during urinary tract infections. *PLoS pathogens* **18**, e1010950, doi:10.1371/journal.ppat.1010950 (2022).

5 Rosen, D. A., Hooton, T. M., Stamm, W. E., Humphrey, P. A. & Hultgren, S. J. Detection of intracellular bacterial communities in human urinary tract infection. *PLoS Med* **4**, e329, doi:10.1371/journal.pmed.0040329 (2007).

6 Anderson, G. G. *et al.* Intracellular bacterial biofilm-like pods in urinary tract infections. *Science* **301**, 105-107, doi:10.1126/science.1084550 (2003).

7 Justice, S. S. *et al.* Differentiation and developmental pathways of uropathogenic Escherichia coli in urinary tract pathogenesis. *Proceedings of the National Academy of Sciences of the United States of America* **101**, 1333-1338, doi:10.1073/pnas.0308125100 (2004).

8 Krogfelt, K. A., Poulsen, L. K. & Molin, S. Identification of coccoid Escherichia coli BJ4 cells in the large intestine of streptomycin-treated mice. *Infect Immun* **61**, 5029-5034, doi:10.1128/iai.61.12.5029-5034.1993 (1993).

9 Andersen, T. E. *et al.* Escherichia coli uropathogenesis in vitro: invasion, cellular escape, and secondary infection analyzed in a human bladder cell infection model. *Infect Immun* **80**, 1858-1867, doi:10.1128/IAI.06075-11 (2012).

10 Söderström, B., Pittorino, M. J., Daley, D. O. & Duggin, I. G. Assembly dynamics of FtsZ and DamX during infection-related filamentation and division in uropathogenic E. coli. *Nature communications* **13**, 3648, doi:10.1038/s41467-022-31378-1 (2022).

11 Iosifidis, G. & Duggin, I. G. Distinct Morphological Fates of Uropathogenic Escherichia coli Intracellular Bacterial Communities: Dependency on Urine Composition and pH. *Infect Immun* **88**, doi:10.1128/IAI.00884-19 (2020).

12 Ong, C. L. *et al.* Identification of type 3 fimbriae in uropathogenic Escherichia coli reveals a role in biofilm formation. *Journal of bacteriology* **190**, 1054-1063, doi:10.1128/JB.01523-07 (2008).

13 Cameron, T. A. & Margolin, W. Insights into the assembly and regulation of the bacterial divisome. *Nature Reviews Microbiology*, 1-13, doi:10.1038/s41579-023-00942-x (2023).

14 Söderström, B., Chan, H., Shilling, P. J., Skoglund, U. & Daley, D. O. Spatial separation of FtsZ and FtsN during cell division. *Molecular microbiology* **107**, 387-401, doi:10.1111/mmi.13888 (2018).

15 Söderström, B. *et al.* Coordinated disassembly of the divisome complex in Escherichia coli. *Molecular microbiology* **101**, 425-438, doi:10.1111/mmi.13400 (2016).

16 Justice, S. S., Hunstad, D. A., Seed, P. C. & Hultgren, S. J. Filamentation by Escherichia coli subverts innate defenses during urinary tract infection. *Proceedings of the National Academy of Sciences of the United States of America* **103**, 19884-19889, doi:10.1073/pnas.0606329104 (2006).

17 Peterson, E. *et al.* The role of bacterial size, shape and surface in macrophage engulfment of uropathogenic E. coli cells. *bioRxiv*, 2022.2011.2020.517300, doi:10.1101/2022.11.20.517300 (2022).

18 Khandige, S. *et al.* DamX Controls Reversible Cell Morphology Switching in Uropathogenic Escherichia coli. *mBio* **7**, doi:10.1128/mBio.00642-16 (2016).

19 Rowlett, V. W. & Margolin, W. The Min system and other nucleoid-independent regulators of Z ring positioning. *Frontiers in microbiology* **6**, 478, doi:10.3389/fmicb.2015.00478 (2015).

20 Fischer-Friedrich, E., Meacci, G., Lutkenhaus, J., Chate, H. & Kruse, K. Intra- and intercellular fluctuations in Min-protein dynamics decrease with cell length. *Proceedings of the National Academy of Sciences of the United States of America* **107**, 6134-6139, doi:10.1073/pnas.0911708107 (2010).

21 Adler, H. I., Fisher, W. D., Cohen, A. & Hardigree, A. A. MINIATURE escherichia coli CELLS DEFICIENT IN DNA. *Proceedings of the National Academy of Sciences of the United States of America* **57**, 321-326, doi:10.1073/pnas.57.2.321 (1967).

22 de Boer, P. A., Crossley, R. E. & Rothfield, L. I. A division inhibitor and a topological specificity factor coded for by the minicell locus determine proper placement of the division septum in E. coli. *Cell* **56**, 641-649, doi:10.1016/0092-8674(89)90586-2 (1989).

23 Bernhardt, T. G. & de Boer, P. A. SlmA, a nucleoid-associated, FtsZ binding protein required for blocking septal ring assembly over Chromosomes in E. coli. *Mol Cell* **18**, 555-564, doi:10.1016/j.molcel.2005.04.012 (2005).

24 Di Ventura, B. & Sourjik, V. Self-organized partitioning of dynamically localized proteins in bacterial cell division. *Molecular systems biology* **7**, 457, doi:10.1038/msb.2010.111 (2011).

25 Corbin, B. D., Yu, X. C. & Margolin, W. Exploring intracellular space: function of the Min system in round-shaped Escherichia coli. *EMBO J* **21**, 1998-2008, doi:10.1093/emboj/21.8.1998 (2002).

26 Hunstad, D. A. & Justice, S. S. Intracellular lifestyles and immune evasion strategies of uropathogenic Escherichia coli. *Annu Rev Microbiol* **64**, 203-221, doi:10.1146/annurev.micro.112408.134258 (2010).

27 Klumpp, D. J. *et al.* Uropathogenic Escherichia coli potentiates type 1 pilus-induced apoptosis by suppressing NF-kappaB. *Infect Immun* **69**, 6689-6695, doi:10.1128/IAI.69.11.6689-6695.2001 (2001).

28 Vaudaux, P. & Waldvogel, F. A. Gentamicin antibacterial activity in the presence of human polymorphonuclear leukocytes. *Antimicrobial agents and chemotherapy* **16**, 743-749, doi:10.1128/aac.16.6.743 (1979).

29 Ducret, A., Quardokus, E. M. & Brun, Y. V. MicrobeJ, a tool for high throughput bacterial cell detection and quantitative analysis. *Nat Microbiol* **1**, 16077, doi:10.1038/nmicrobiol.2016.77 (2016).

30 Wissel, M. C. & Weiss, D. S. Genetic analysis of the cell division protein FtsI (PBP3): amino acid substitutions that impair septal localization of FtsI and recruitment of FtsN. *Journal of bacteriology* **186**, 490-502 (2004).